Mineralogical Magazine (2023), **87**, 60–68
doi:10.1180/mgm.2022.114

CAMBRIDGE UNIVERSITY PRESS

Article

Magnesio-lucchesiite from the Kowary vicinity, Karkonosze Mountains, SW Poland: the third occurrence worldwide

Mateusz P. Sęk[1]*, Adam Włodek[1], Marcin Stachowicz[2], Krzysztof Woźniak[3] and Adam Pieczka[1]

[1]Department of Mineralogy, Petrography and Geochemistry, AGH University of Science and Technology, Mickiewicza 30, 30-059 Kraków, Poland; [2]University of Warsaw, Faculty of Geology, 02-089 Warszawa, Żwirki and Wigury 93, Poland; and [3]University of Warsaw, Department of Chemistry, 02-093 Warszawa, Pasteura 1, Poland

Abstract

Two tourmaline samples occurring in quartz veinlets, which cross-cut an amphibolite body at the Budniki camp near the Kowary town in the south-west part of the Karkonosze Mountains, SW Poland, were studied through microprobe and single crystal X-ray diffraction. Samples were extracted from core and rim regions of crystals with concentric zoning. Chemical and structural data revealed that the core tourmaline is characterised by a dravite–oxy-dravite composition, with the formula: $^{X}(Na_{0.82}Ca_{0.07}K_{0.01}Sr_{0.01}\square_{0.09})_{\Sigma1}{}^{Y}(Mg_{1.73}Fe^{2+}_{0.81}Fe^{3+}_{0.41}Ti_{0.04}V_{0.01})_{\Sigma3}{}^{Z}(Al_{5.85}Fe^{3+}_{0.15})_{\Sigma6}({}^{T}Si_6O_{18})(BO_3)_3(OH)_3{}^{W}(OH_{0.50}O_{0.50})_{\Sigma1}$ and unit cell parameters $a = 15.97377(14)$ Å and $c = 7.22644(7)$ Å. The rim part of the crystals has a magnesio-lucchesiite composition, described by the formula: $^{X}(Ca_{0.49}Na_{0.41}K_{0.04}Sr_{0.02}\square_{0.04})_{\Sigma1}{}^{Y}(Mg_{1.87}Fe^{2+}_{0.95}Ti_{0.15}Fe^{3+}_{0.02}V_{0.02})_{\Sigma3}{}^{Z}(Al_{5.49}Fe^{3+}_{0.51})_{\Sigma6}(BO_3)_3({}^{T}Si_6O_{18})(OH)_3{}^{W}(O_{0.81}F_{0.18}OH_{0.01})_{\Sigma1}$ with unit cell parameters $a = 15.9863(3)$ Å and $c = 7.22426(15)$ Å. Both tourmalines show similar refined populations at the Y and Z sites: $^{Y}[(Fe^{2+}_{0.810}Mg_{0.680})_{\Sigma1.490}(Al_{1.044}Fe^{3+}_{0.413}V_{0.009})_{\Sigma1.465}Ti_{0.045}]_{\Sigma3}{}^{Z}(Al_{4.806}Mg_{1.042}Fe^{3+}_{0.152})_{\Sigma6}$ (dravite–oxy-dravite), and $^{Y}[(Fe^{2+}_{0.945}Mg_{0.750})_{\Sigma1.695}(Al_{0.737}Fe^{3+}_{0.404}V_{0.018})_{\Sigma1.159}Ti_{0.146}]_{\Sigma3}{}^{Z}(Al_{4.749}Mg_{1.115}Fe^{3+}_{0.137})_{\Sigma6}$ (magnesio-lucchesiite), with a comparable Mg/(Mg + Fe) ratio of ~0.54–0.56, oxidation of Fe expressed as Fe^{3+}/Fe_{total} ratio ~0.36–0.41, and trace components such as Ti, Sr, V, Cr, Ni and Co. The geological history of the eastern Karkonosze region in the Kowary vicinity indicates that both tourmalines crystallised from B-bearing metamorphic fluids mobilised by Variscan prograde metamorphism from the protoliths of the Velká Upá mica schists that host the Budniki amphibolite. The fluids migrated into the tectonised amphibolite enriched in Ti, V, Cr, Ni and Co, and mineralised the fractures within it through deposition of soluble species in the form of quartz–tourmaline veinlets. Magnesio-lucchesiite crystallised in an early retrogression stage, probably from Ca- and F-bearing fluids secondary enriched in B by the dissolution of dravite–oxy-dravite. The Budniki camp is, in addition to the type and co-type magnesio-lucchesiite localities, the third documented occurrence of the species worldwide.

Keywords: magnesio-lucchesiite, oxy-dravite, dravite, tourmaline, structure refinement

(Received 1 July 2022; accepted 28 September 2022; Accepted Manuscript published online: 14 October 2022; Associate Editor: Giancarlo Della Ventura)

Introduction

Minerals of the tourmaline supergroup are (Si_6O_{18})-ring borosilicates with very diversified compositions. They occur as minor to accessory minerals in low-grade to ultrahigh-pressure metamorphic rocks, granites and granitic pegmatites, as chemically resistant phases in sedimentary rocks, and as common gangue minerals in diverse types of hydrothermal deposits (e.g. Ertl *et al.*, 2010; Slack and Trumbull, 2011; van Hinsberg *et al.*, 2011; Henry and Dutrow, 2012; Biernacka, 2019). According to Henry *et al.* (2011), the general chemical formula of the tourmaline supergroup minerals can be written as $XY_3Z_6(T_6O_{18})(BO_3)_3V_3W$, where the populations of cations and anions at specific structural sites are indicated in capital letters: $^{IX}X = Na^+$, K^+, Ca^{2+}, Pb^{2+} and $\square$ ($\square$ = vacancy); $^{VI}Y = Fe^{2+}$, Mg^{2+}, Mn^{2+}, Al^{3+}, Li^+, Fe^{3+}, Cr^{3+}, V^{3+}, Ti^{4+}, Zn^{2+}, Cu^{2+} and Ni^{2+}; $^{VI}Z = Al^{3+}$, Fe^{3+}, Cr^{3+}, V^{3+}, Mg^{2+} Fe^{2+} and Ti^{4+}; $^{IV}T = Si^{4+}$, Al^{3+} and B^{3+}; $^{III}B = B^{3+}$; $^{III,IV}V = OH^-$ and O^{2-}; and $^{III,IV}W = OH^-$, F^- and O^{2-}. The dominant occupant at the X site determines the affiliation of a tourmaline to one of the three groups: alkali, calcic and X-vacant, whereas the occupation of the W site determines the fluor-, hydroxyl- and oxy-tourmaline species. Tourmalines are known for their wide *P–T* stability range up to UHP conditions as well as their complex chemical composition with negligible diffusion of elements. All these aspects make them efficient geological tools for investigating *P–T–X* conditions during their formation, being excellent petrogenetic indicators (e.g. Henry and Guidotti, 1985; Henry and Dutrow, 1996; van Hinsberg *et al.*, 2011; Berryman *et al.*, 2015, 2016; Dutrow and Henry, 2016).

There are 18 oxy-tourmaline species (Pasero, 2022). One of these oxy-species is magnesio-lucchesiite, originally known from only two occurrences in Canada and Italy (Scribner *et al.*, 2021). Crystals of magnesio-lucchesiite have subsequently been

*Author for correspondence: Mateusz P. Sęk, Email: msek@agh.edu.pl
Cite this article: Sęk M.P., Włodek A., Stachowicz M., Woźniak K. and Pieczka A. (2023) Magnesio-lucchesiite from the Kowary vicinity, Karkonosze Mountains, SW Poland: the third occurrence worldwide. *Mineralogical Magazine* **87**, 60–68. https://doi.org/10.1180/mgm.2022.114

found within quartz veins cross-cutting an amphibolite body in proximity of the Kowary town, SE Karkonosze-Izera Massif, south-western Poland, ~1 km to west of the oxy-dravite occurrence on Wołowa Góra Mt. (Pieczka *et al.*, 2018), thus representing the third documented occurrence of magnesio-lucchesiite worldwide. This work addresses the chemical and structural characterisation of this peculiar oxy-tourmaline species. In this study we also provide a brief discussion on the crystallisation environment in which this tourmaline species was formed.

Geological setting

The Kowary area, where the tourmaline samples were collected, belongs to the Izera–Kowary Unit in the southeastern part of the Karkonosze–Izera Massif, Western Sudetes, Poland, in the northeast periphery of the Bohemian Massif (Fig. 1a). The Karkonosze–Izera Massif includes a core intrusion of Variscan granite ~320–315 Ma (Machowiak and Armstrong, 2007; Kryza *et al.*, 2014; Kusiak *et al.*, 2014) surrounded by a Neoproterozoic–Palaeozoic metamorphic envelope with a sequence of four distinct units: (l) the Izera–Kowary Unit in the north and south-east along with the Velká Upá Group (leucogranites, gneisses, mica schists, mafic and felsic metavolcanics, graphite quartzites, hornfelses and marbles); (2) the Ješted Unit exposed in the south-west (weakly metamorphosed sediments and minor volcanics, marbles, metasandstones, phyllites and metaconglomerates); (3) the South Karkonosze Unit in the south (gneisses, mica schists, phyllites, metasedimentary rocks and basic and felsic metavolcanic rocks); and (4) the Leszczyniec Unit on the east (felsic gneisses, mica schists, amphibolites, phyllites and marbles) (Mazur, 1995; Mazur *et al.*, 2006). The units are interpreted as a nappe structure formed from mixed magmatic–sedimentary protoliths connected with pre-Variscan bimodal volcanism related to the development of the continental rift (e.g. Oberc-Dziedzic *et al.*, 2005, 2010; Mazur *et al.*, 2006; Pin *et al.*, 2007). Rocks of the Izera–Kowary Unit, the closest to the Karkonosze granite, are represented by Izera, Karkonosze and Kowary orthogneisses with their granitic protoliths dated at 515–480 Ma (Borkowska *et al.*, 1980; Korytowski *et al.*, 1993; Oliver *et al.*, 1993; Kröner *et al.*, 2001), and the Velká Upá Group schist series considered as the country rocks to the ~500 Ma granite protoliths of the orthogneisses, metamorphosed under upper greenschist- to lower amphibolite-facies conditions. They often contain small intercalations of mafic and felsic meta-igneous rocks representing bimodal volcanic activity (Żaba, 1984; Oberc-Dziedzic, 1988; Kryza and Mazur, 1995; Mazur *et al.*, 2006; Mochnacka *et al.*, 2008; Oberc-Dziedzic *et al.*, 2010; Ilnicki, 2011).

The tourmalines studied originate from quartz veinlets within an amphibolite body hosted by mica schists of Czoło Mt., in the so-called Budniki camp near Kowary town in the Polish part of the Karkonosze Mountains, which were cross-cut by a prospect adit for uranium during searches in the area in the 1950s (Fig. 1b). The remains of the excavated material are still accessible in a small waste dump in the Malina stream along the green tourist route from Karpacz to the Okraj Pass in the Kowary range. The samples of amphibolite with tourmaline–quartz veinlets from the dump contain locally scattered Ti-bearing and Fe–Cu–Ni–Co–Zn–Pb-sulfide–sulfoarsenide mineralisation formed by ilmenite, rutile, titanite, pyrrhotite, pyrite, arsenopyrite, chalcopyrite, sphalerite, galena, cobaltite, gersdorffite, marcasite, pentlandite and traces of scheelite and wolframite (Mochnacka *et al.*, 2008).

Methods

Electron-probe microanalysis

Quantitative chemical analyses of the tourmalines were done using a JEOL SuperProbe JXA-8230 electron microprobe at the Laboratory of Critical Elements AGH–KGHM, Faculty of Geology, Geophysics and Environmental Protection, AGH University of Science and Technology, Kraków, Poland. The microprobe operated in wavelength-dispersive X-ray spectrometry (WDS) mode with a 15 kV accelerating voltage, 20 nA beam current and 5 μm beam size. Standards, diffracting crystals, analytical lines and detection limits (element wt.%) were as follows: fluorite – F (LDE1, *K*α, 0.04), albite – Na (TAP, *K*α, 0.02), Si (TAP, *K*α, 0.03), Al (TAP, *K*α, 0.04); diopside – Mg (TAP, *K*α, 0.03) and Ca (PET, *K*α, 0.02); fayalite – Fe (LIF, *K*α, 0.04); rhodonite – Mn (LIF, *K*α, 0.05); synthetic NiO – Ni (LIFL, *K*α, 0.04); chromite – Cr (PET, *K*α,0.04); V_2O_3 – V (PET, *K*α, 0.01); willemite – Zn (LIF, *K*α, 0.05); Sc_2O_3 – Sc (PET, *K*α, 0.01); sanidine – K (PET, *K*α, 0.01); and rutile – Ti (PET, *K*α, 0.02). Raw data were reduced with the ZAF routine. Due to a small excess of Si in microprobe determinations, the atom contents in the tourmaline formulae were normalised on the basis of (Y + Z) site occupants equal to 9 atoms per formula unit (apfu), and the Si content was accepted as 6 apfu. B_2O_3 and H_2O were calculated based on the tourmaline stoichiometry with the assumption of B = 3 apfu, and H_2O occurring as OH groups from charge-balanced formulae. As it was not possible to determine directly the content of FeO and Fe_2O_3 (e.g. using Mössbauer spectroscopy), as well as the amount of H_2O, and considering that the relationship among the constituents Fe^{2+}–Fe^{3+} and OH–O depends on the coupled substitution $Fe^{2+} + OH^- = Fe^{3+} + O^{2-}$, the results of analysis of the difference-Fourier maps and the structure refinement were taken into account. These analyses indicated the presence of H atoms bonded to O(3) oxygen atoms at the V sites of both crystals, and no distinct q-peaks in the immediate vicinity of the W sites that could be related to H at the H1 site (bonded to O(1)) at the tourmaline rim. Thus, for both the tourmaline crystals studied, the Fe^{3+}/Fe_{total} ratio was matched in order to obtain identical calculated <Y–O> and <Z–O> distances to the values refined in the structural analysis, using site-scattering values optimised on the basis of the results of microprobe determination and structure refinement. The optimisation of the Fe^{3+}/Fe_{total} ratio on the basis of the comparison of Y and Z site bond-valence sums with average charges of the site occupants (e.g. Scribner *et al.*, 2021), although initially considered, was not carried out due to insignificant differences among the parameters.

Single-crystal X-ray structural studies and refinement

X-ray diffraction (XRD) data from single crystals were collected using a SuperNova four-circle diffractometer equipped with an HyPix Hybrid Pixel Array Detector (Rigaku Oxford Diffraction). The crystal-to-detector distance was 54.9 mm. Cu*K*α radiation (λ = 1.54184 Å) was used at 50 kV and 0.8 mA. Crystal fragments of sizes 0.055 × 0.026 × 0.011 mm (core tourmaline) and 0.050 × 0.043 × 0.022 mm (rim tourmaline) were mounted on a non-diffracting carbon fibre of 0.01 mm diameter, which was attached to a steel pin support. A frame-width of 0.5° in ω scans and frame times set to 17.79 and 71.16 s for the crystal extracted from the tourmaline rim (magnesio-lucchesiite) and 1.20, 5.00 and 6.00 s for the crystal from the tourmaline core (dravite–oxy-dravite), were used.

https://doi.org/10.1180/mgm.2022.114 Published online by Cambridge University Press

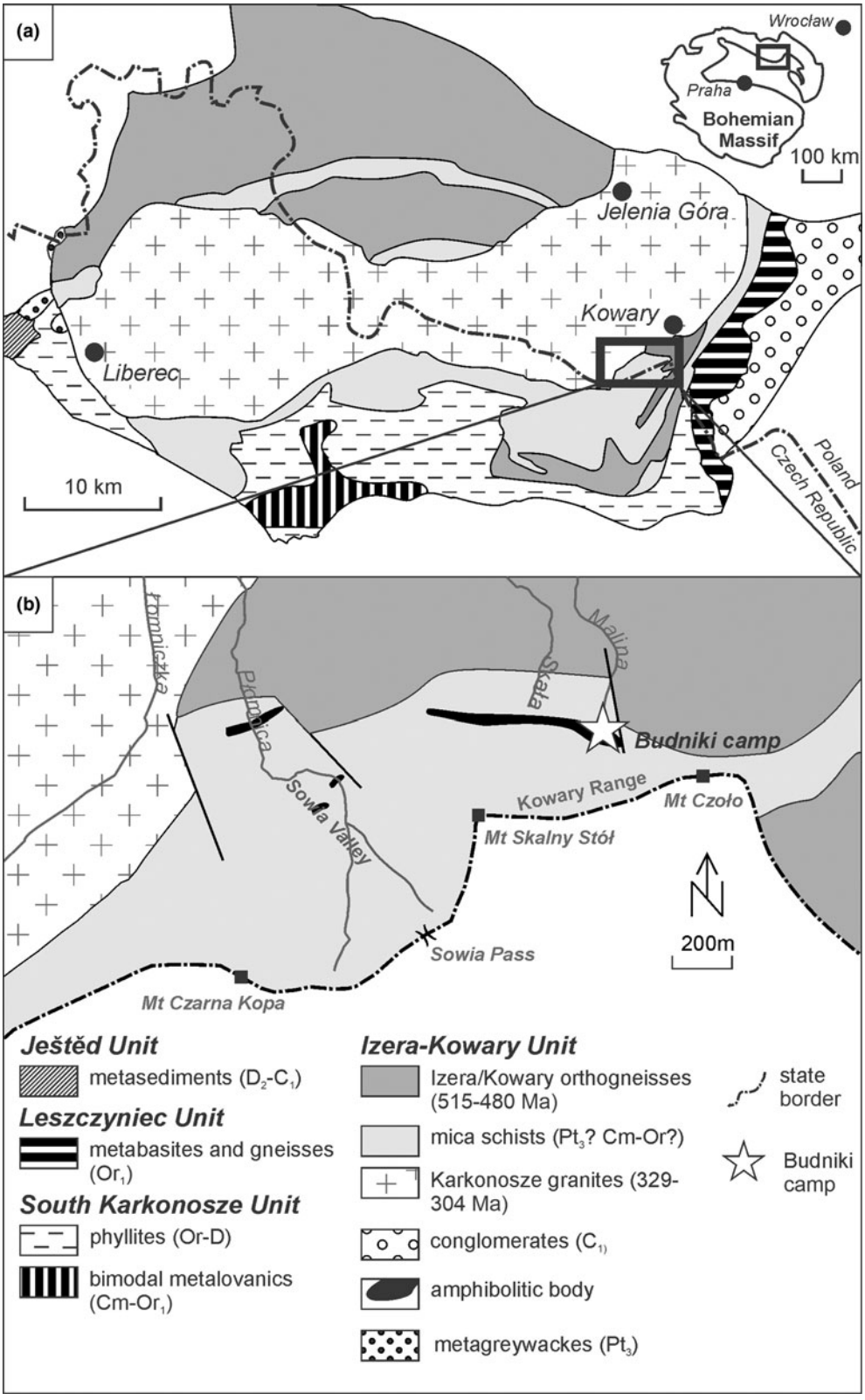

Fig. 1. Geological sketch map: (a) of the Karkonosze-Izera massif (after Ilnicki, 2011); (b) southeastern metamorphic envelope in the Kowary area.

Crystal structures were solved with the dual-space iterative phasing algorithm implemented in *ShelXT* (Sheldrick, 2015a) that located all positions of cations (except hydrogen) and O anions. The correct element assignment for cations and anions was based on compositional data obtained by EMPA and crystal-chemical reasoning, comprising site-scattering, coordination and bond lengths. The model was refined with the least squares minimisation using *Shelxl* (Sheldrick, 2015b), within *Olex2*

https://doi.org/10.1180/mgm.2022.114 Published online by Cambridge University Press

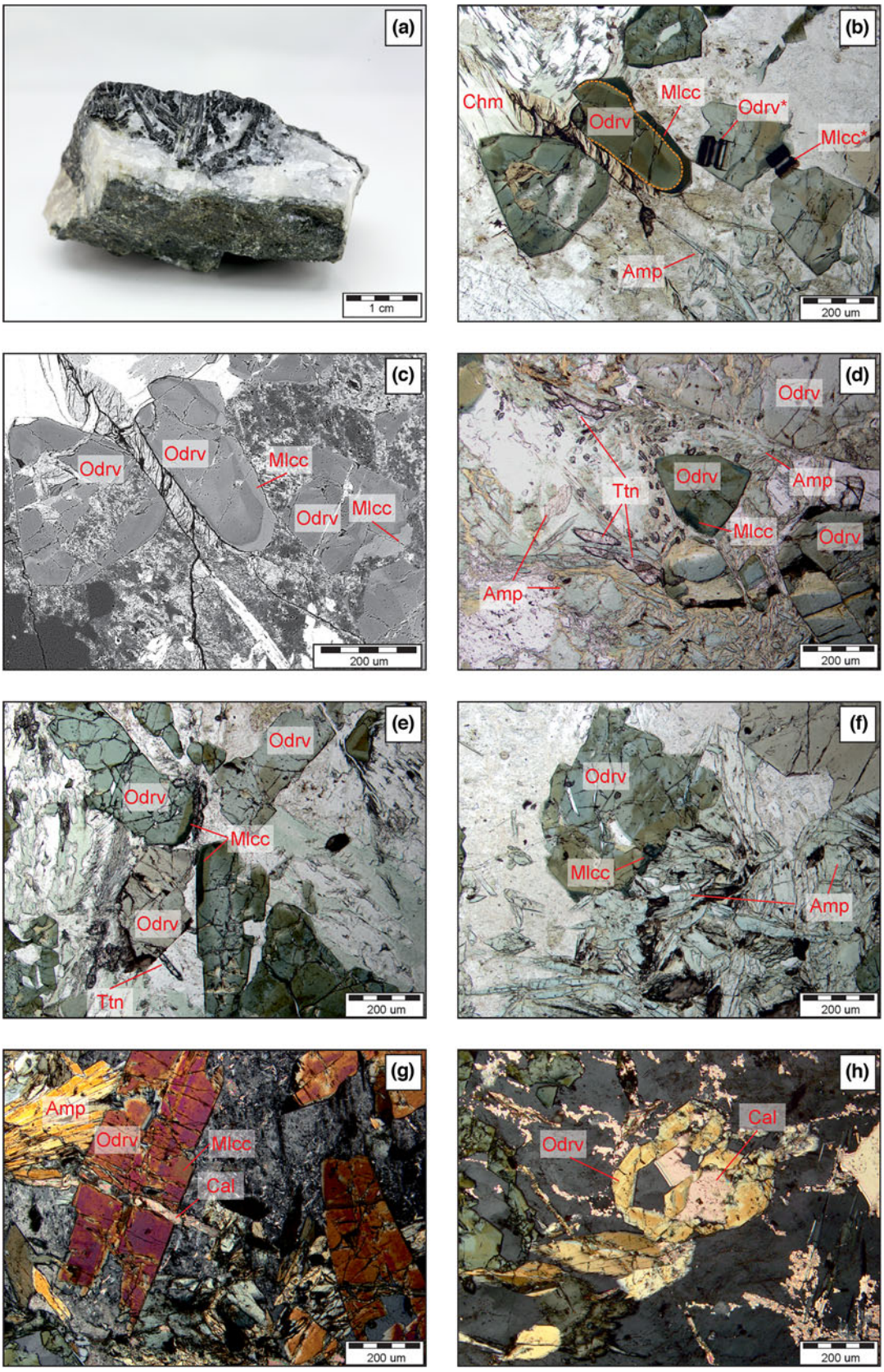

Fig. 2. Internal texture of quartz-tourmaline veins hosted by the Budniki amphibolite. (a) Representative hand specimen of the quartz-tourmaline vein. (b and d–f) Optical images of zoned tourmaline forming intergrowths with amphiboles, titanite and chlorite (transmitted polarised light). Extraction sites of crystals used in single-crystal X-ray diffraction are marked with abbreviations Odrv* and Mlcc* in Fig. 1b. The core / rim border in a crystal of the Budniki tourmaline is marked by an orange dashed line in the same figure. (c) A back-scattered-electron image of the crystals appropriate for the extraction. (g,h) Optical images of the vein tourmalines locally associated with calcite (transmitted light, crossed polars). Mineral name abbreviations: Amp – amphibole, Cal- calcite, Chm – chamosite, Mlcc – magnesio-lucchesiite, Odrv – oxy-dravite, Tnt – titanite (Warr, 2021).

https://doi.org/10.1180/mgm.2022.114 Published online by Cambridge University Press

Table 1. Representative compositions of dravite–oxy-dravite and magnesio-lucchesiite from Budniki.*

	Dravite–oxy-dravite		Magnesio-lucchesiite	
wt.%	Measured $n = 3$	Optimised	Measured $n = 3$	Optimised
SiO_2	36.03(2)	36.03	35.57(33)	35.57
TiO_2	0.55(15)	0.35	1.14(25)	1.14
$B_2O_{3(calc.)}$		10.27		10.16
Al_2O_3	28.95(12)	29.31	26.52(68)	27.20
V_2O_3	0.06(0)	0.06	0.13(2)	0.13
$Fe_2O_{3(calc.)}$		4.44		4.20
FeO	10.16(11)	5.72	10.86(42)	6.60
MgO	6.12(24)	6.84	7.18(13)	7.31
CaO	0.38(3)	0.38	2.67(34)	2.67
SrO	0.11(2)	0.11	0.22(7)	0.22
Na_2O	2.51(12)	2.51	1.25(18)	1.25
K_2O	0.04(1)	0.04	0.16(10)	0.16
$H_2O_{(calc.)}$		3.10		2.63
F	b.d.l.	0.00	0.22(6)	0.34
$-O = F_2$	0.00	0.00	−0.09	−0.14
Total	84.91	99.15	85.83	99.43
Apfu				
Si^{4+}		6.000		6.000
Ti^{4+}		0.045		0.146
B^{3+}		3.000		3.000
Al^{3+}		5.847		5.486
V^{3+}		0.009		0.018
Fe^{3+}		0.565		0.541
Fe^{2+}		0.810		0.945
Mg^{2+}		1.726		1.865
Ca^{2+}		0.068		0.490
Sr^{2+}		0.011		0.021
Na^{+}		0.823		0.414
K^{+}		0.008		0.036
F^{-}		0.000		0.184
$(OH)^{-}$		3.501		3.006
O^{2-}		27.499		27.810

*Notes: Mn, Cr and Zn are below detection limits (b.d.l.), n = number of spot analyses. Data in parentheses are estimated standard deviations.

(Dolomanov *et al.*, 2009) as a graphical interface. When more than one element occupied the same position in the asymmetric unit, constraints for equal atom coordinates and equal anisotropic displacement parameters for these groups of atoms within each unique site were applied. The occupancies of X, Y and Z sites in both analysed crystals were refined. In details, the occupancies of the Y and Z sites were refined as Fe *vs.* Mg and fractional occupancy of Al, respectively. The latter converged to 1.000(6) and 0.998(7) in core and rim tourmaline, respectively. Thus, in the final refinement values of the parameter were fixed to 1. The W site occupancy was constrained to 1 and refined as F *vs.* O in the rim tourmaline, and fixed to 1 with the oxygen form factor in the core tourmaline. The X site occupancy was refined as fractional occupancies of Na *vs.* vacancy for tourmaline forming the core, and Na *vs.* Ca for the rim tourmaline, respectively. The T- and B-site occupancies were fixed as $Si_{1.00}$ and $B_{1.00}$.

Results

Chemical composition

The tourmalines studied are representative of the core and rim regions of crystals characterised by concentric zoning, occurring in quartz veinlets of 1–5 cm in thickness cutting an amphibolite body in the Malina stream valley, Karkonosze Mountains. The crystals are black in hand specimen, reach up to 15 mm in length and 3–4 mm in diameter, locally form massive accumulations in the vein quartz, and sometimes are associated with alkali feldspars, chamosite, titanite, ilmenite and base-metal sulfides (Fig. 2a). In thin section, the tourmaline crystals show concentric zoning with a greenish to brown coloured core, with less frequent complex intersector zoning typical for metamorphic tourmalines described by Van Hinsberg *et al.* (2006) (Fig. 2b–h). The core tourmaline has been partly leached and overgrown by a discontinuous rim of a younger tourmaline with a dark green ω pleochroic colour (Fig. 2b–f). The quartz veinlets are cracked due to tectonic stress, and resealed with calcite and rarely fluorite crystals (Fig. 2g,h).

Electron probe microanalysis (EPMA) data is given in Table 1, with optimised compositions of both tourmaline crystals, averaged from three spot analyses for each zone. The calculated B_2O_3, H_2O, FeO and Fe_2O_3 amounts are derived on the basis of the EPMA and structure refinement (SREF) results. According to Henry *et al.* (2011), the resulting empirical ordered formulae for core tourmaline samples is: $^{X}(Na_{0.82}Ca_{0.07}K_{0.01}Sr_{0.01}\square_{0.09})_{\Sigma1}$ $^{Y}(Mg_{1.73}Fe^{2+}_{0.81}Fe^{3+}_{0.41}Ti_{0.04}V_{0.01})_{\Sigma3}$ $^{Z}(Al_{5.85}Fe^{3+}_{0.15})_{\Sigma6}$ (Si_6O_{18}) $(BO_3)_3(OH)_3$ $^{W}OH_{0.50}O_{0.50})_{\Sigma1}$, and for rim tourmaline is: $^{X}(Ca_{0.49}Na_{0.41}K_{0.04}Sr_{0.02}\square_{0.04})_{\Sigma1}$ $^{Y}(Mg_{1.86}Fe^{2+}_{0.94}Ti_{0.15}Fe^{3+}_{0.03}V_{0.02})_{\Sigma3}$ $^{Z}(Al_{5.49}Fe^{3+}_{0.51})_{\Sigma6}$ $(^{T}Si_6O_{18})(BO_3)_3(OH)_3$ $^{W}(O_{0.81}F_{0.18}OH_{0.01})_{\Sigma1}$.

The idealised empirical formula of the core tourmaline, $Na(Mg_{2.5}Fe^{3+}_{0.5})Al_6(BO_3)_3(Si_6O_{18})(OH)_3(OH_{0.5}O_{0.5})$, corresponds to the mid-member in the solid-solution series between dravite, $NaMg_3Al_6(BO_3)_3(Si_6O_{18})(OH)_3(OH)$, and a ferric-analogue (Fe^{3+} replaces ^{Y}Al) of oxy-dravite, $Na(Mg_2Fe^{3+})Al_6(BO_3)_3(Si_6O_{18})(OH)_3O$. The rim tourmaline is magnesio-lucchesiite, $CaMg_3Al_6(BO_3)_3(Si_6O_{18})(OH)_3O$, as it is Ca-dominant at the X position in the general formula of tourmaline, ^{Y}Mg- and ^{Z}Al-dominant, and oxy-dominant at W with O^{2-} > (OH + F). It forms a solid solution with dutrowite, $Na(Fe^{2+}_{2.5}Ti_{0.5})Al_6(BO_3)_3(Si_6O_{18})(OH)_3O$. Both tourmalines differ generally in Ca + Sr contents (0.068 Ca and 0.011 Sr apfu in the core dravite–oxy-dravite *vs.* 0.490 Ca and 0.021 Sr apfu in the rim magnesio-lucchesiite) at the X-site, and the W-site occupants (O, OH and F) where O^{2-} is the dominant occupant only in magnesio-lucchesiite (0.810 apfu); F is also detected by EPMA in this species (0.184 apfu; Table 1). The $Mg/(Mg + Fe_{total})$ ratio of 0.556 in dravite–oxy-dravite and 0.541 in magnesio-lucchesiite, indicates close genetic affinity of the two tourmaline species in the crystals. Overall, the composition of the Budniki tourmalines is formed by three substitutions: (1) $^{X}Na^{+} + {}^{W}OH^{-} \leftarrow {}^{X}Ca^{2+} + {}^{W}O^{2-}$; (2) isovalent anionic $^{W}OH^{-} \leftarrow {}^{W}F$; and (3) deprotonation: $^{Y}(Mg,Fe)^{2+} + {}^{W}OH^{-} \leftarrow {}^{Y}Fe^{3+} + {}^{W}O^{2-}$ and $^{Y}(Mg,Fe)^{2+} + 2{}^{W}OH^{-} \leftarrow {}^{Y}Ti^{4+} + 2{}^{W}O^{2-}$.

Crystal structure

Crystal, data-collection and refinement details are presented in Table 2. Atomic coordinates, equivalent displacement parameters, and refined occupancy for atomic sites are shown in Table 3. Anisotropic displacement parameters for both the crystals are accessible in the crystallographic information file, which has been deposited with the Principal Editors of *Mineralogical Magazine* and is available as Supplementary material. Selected bond lengths are collected in Table 4, assigned site populations are reported in Table 5, and calculated bond valences are shown in Table 6.

https://doi.org/10.1180/mgm.2022.114 Published online by Cambridge University Press

Table 2. Crystal information and details of X-ray diffraction data collection and refinement for magnesio-lucchesiite and dravite–oxy-dravite.

	Magnesio-lucchesiite	Dravite–oxy-dravite
Crystal data		
Ideal formula	$CaMg_3Al_6(BO_3)_3(Si_6O_{18})(OH)_3O$	$Na(Mg_{2.5}Fe^{3+}_{0.5})Al_6(BO_3)_3(Si_6O_{18})(OH)_3(OH_{0.5}O_{0.5})$
Crystal chemical formula	$Al_6B_3Ca_{0.56}F_{0.21}Fe_{1.48}H_3Mg_{1.52}Na_{0.44}O_{30.79}Si_6$	$Al_6B_3Ca_{0.05}Fe_{1.29}H_3Mg_{1.71}Na_{0.95}O_{31}Si_6$
Crystal dimensions (mm)	0.043 × 0.022 × 0.05	0.055 × 0.026 × 0.011
Crystal system, space group	trigonal, *R*3*m*	trigonal, *R*3*m*
Temperature (K)	292.6(9)	292(1)
a, *c* (Å)	15.9863(3), 7.22426(15)	15.97377(14), 7.22644(7)
V (Å^3)	1598.89(6)	1596.87(3)
Z	3	3
Calculated density (g cm^{-3})	3.162	3.117
μ (mm^{-1})	17.75	15.251
Data collection		
Crystal description	plate	plate
Instrument	SuperNova X-ray Source, HyPix detector	
Radiation type, wavelength (Å)	Cu*K*α, λ = 1.54184	
Number of frames	3430	10034
θ range (°)	5.535–77.616	5.539–77.763
Absorption correction	multi-scan	multi-scan
T_{min}, T_{max}	0481, 0.704	0.488, 0.850
No. of measured, independent and observed [$I > 2\sigma(I)$] reflections	3753, 786, 779	11293, 845, 842
R_{int}	0.0333	0.0289
Data completeness	to θ = 67.684° 100% to θ = 77.616° 98.4%	to θ = 67.684° 100% to θ = 77.763° 99.08%
Indices range of *h*, *k*, *l*	$-18 \le h \le 20$, $-20 \le k \le 19$, $-9 \le l \le 8$	$-20 \le h \le 20$, $-20 \le k \le 20$, $-9 \le l \le 9$
Refinement details		
Number of reflections, parameters, restraints	786, 95, 2	845, 95, 2
R_1 [$I > 2\sigma(I)$], R_1(all)	0.0187, 0.0189	0.0153, 0.0154
wR_2 [$I > 2\sigma(I)$], wR_2(all)	0.0501, 0.0502*	0.0394, 0.0394#
GoF	1.069	1.124
Flack parameter	0.013(7)	0.014(5)
$\Delta\rho_{max}$, $\Delta\rho_{min}$ (e^- Å^{-3})	0.29, −0.26	0.21, −0.34

*$w = 1/[\sigma^2(F_o^2) + (0.040P)^2]$; #$w = 1/[\sigma^2(F_o^2) + (0.0295P)^2 + 0.6222P]$, where $P = (F_o^2 + 2F_c^2)/3$.

Table 3. Atomic coordinates, equivalent displacement parameters, and refined occupancies for atomic sites in the Budniki dravite–oxy-dravite and magnesio-lucchesiite.

Site	Occupant	*x*	*y*	*z*	U_{eq} / U^*_{iso}	Refined occupancy
Dravite–oxy-dravite						
X	Na, Ca	⅓	⅔	0.4293(4)	0.0256(12)	$Na_{0.95(2)}Ca_{0.05(2)}$
Y	Fe, Mg	0.39563(3)	0.60437(3)	0.03302(10)	0.0095(3)	$Fe_{0.430(6)}Mg_{0.570(6)}$
Z	Al	0.59521(5)	0.63006(5)	0.05491(10)	0.00776(17)	1
B	B	0.5534(3)	0.77671(15)	0.2109(5)	0.0097(7)	1
T	Si	0.52323(5)	0.66483(5)	0.66686(10)	0.00776(18)	1
O1 = W	O	⅓	⅔	−0.1073(7)	0.0218(10)	1
O2	O	0.45585(19)	0.72793(10)	0.1812(4)	0.0148(6)	1
O3 = V	O	0.46575(10)	0.53425(10)	0.1545(4)	0.0158(5)	1
O4	O	0.5188(2)	0.75938(10)	0.5971(4)	0.0132(5)	1
O5	O	0.42540(10)	0.57460(10)	0.5766(4)	0.0135(5)	1
O6	O	0.51952(13)	0.65677(13)	−0.1113(3)	0.0118(4)	1
O7	O	0.61797(12)	0.66677(13)	0.5874(2)	0.0122(3)	1
O8	O	0.60321(14)	0.72735(13)	0.2251(3)	0.0133(4)	1
H3	H	0.461(2)	0.539(2)	0.282(4)	0.06(2)*	1
Magnesio-lucchesiite						
X	Na, Ca	⅓	⅔	0.4443(3)	0.0179(9)	$Na_{0.44(2)}Ca_{0.56(2)}$
Y	Fe, Mg	0.39501(4)	0.60499(4)	0.03125(14)	0.0113(3)	$Fe_{0.495(8)}Mg_{0.505(8)}$
Z	Al	0.59496(7)	0.62997(7)	0.05527(13)	0.0088(2)	1
B	B	0.5539(4)	0.77694(19)	0.2151(7)	0.0111(9)	1
T	Si	0.52340(6)	0.66498(6)	0.66720(12)	0.0088(2)	1
O1 = W	O, F	⅓	⅔	−0.1129(10)	0.023(2)	$O_{0.79(13)}F_{0.21(13)}$
O2	O	0.4547(2)	0.72737(12)	0.1895(5)	0.0153(7)	1
O3	O	0.46648(14)	0.53352(14)	0.1551(5)	0.0166(7)	1
O4	O	0.5176(3)	0.75881(13)	0.5953(5)	0.0135(7)	1
O5	O	0.42437(13)	0.57563(13)	0.5765(5)	0.0141(7)	1
O6	O	0.52009(16)	0.65760(16)	−0.1112(4)	0.0126(5)	1
O7	O	0.61733(16)	0.66607(16)	0.5872(3)	0.0133(5)	1
O8	O	0.60323(18)	0.72731(18)	0.2256(3)	0.0142(5)	1
H3	H	0.460(3)	0.540(3)	0.285(5)	0.05(2)*	1

https://doi.org/10.1180/mgm.2022.114 Published online by Cambridge University Press

Table 4. Selected mean bond lengths in dravite–oxy-dravite and magnesio-lucchesiite tourmalines from Budniki.

	Dravite–oxy-dravite	Magnesio-lucchesiite
Na–O2 ×3	2.468(3)	2.493(4)
Na–O5 ×3	2.761(3)	2.695(4)
Na–O4 ×3	2.837(3)	2.775(4)
<Na–O>	2.689	2.654
Y–O1	2.000(3)	2.000(4)
Y–O6 ×2	2.0120(19)	2.021(2)
Y–O2 ×2	2.0171(18)	2.044(3)
Y–O3	2.129(3)	2.172(4)
<Y–O>	2.0312	2.0503
Z–O6	1.898(2)	1.898(3)
Z–O8	1.9012(19)	1.902(3)
Z–O7	1.9051(19)	1.912(3)
Z–O8	1.9355(19)	1.936(3)
Z–O7	1.9673(19)	1.974(2)
Z–O3	1.9929(14)	1.9872(18)
<Z–O>	1.9333	1.9349
B–O2	1.367(5)	1.385(6)
B–O8 ×2	1.376(3)	1.373(3)
<B–O>	1.373	1.377
Si–O7	1.6043(17)	1.601(2)
Si–O6	1.607(2)	1.604(3)
Si–O4	1.6273(10)	1.6329(14)
Si–O5	1.6408(13)	1.6477(17)
<Si–O>	1.6199	1.6214

The crystal structures of the two tourmalines were refined in the space group *R*3*m* (*Z* = 3) to R_1 values of 1.53% (dravite–oxy-dravite) and 1.87% (magnesio-lucchesiite). In the structure of both crystals, the B and T sites are occupied exclusively by B and Si, respectively, as can be deduced from the refined <B–O> and <T–O> mean distances of 1.373(4) and 1.377(4) Å, and 1.620(2) and 1.621(2) Å, respectively (Table 4). The refined X site occupancies: $Na_{0.95(2)}Ca_{0.05(2)}$ in dravite–oxy-dravite and $Ca_{0.56(2)}Na_{0.44(2)}$ in magnesio-lucchesiite (Table 3) correspond to 11.5(2) and 16.0(2) valence units (vu), respectively, versus 11.0 and 15.9 vu, derived from the respective empirical formulae. The sums of bond valences at the site correspond to 0.89 vu in dravite–oxy-dravite and 1.26 vu in magnesio-lucchesiite, which are comparable with averaged valences of the site cations of 0.99 and 1.47 vu (Table 6).

Table 5. Optimised site populations for the tourmalines studied.

Site	Site population	Site scattering (epfu)		Mean bond lengths (Å)	
		SREF	EPMA	SREF	EPMA
	Dravite–oxy-dravite (core)				
X	$Na_{0.823}K_{0.008}Ca_{0.068}Sr_{0.011}\square_{0.090}$	11.5(2)	11.0	2.689(3)	
Y	$Fe^{2+}_{0.810}Mg_{0.680}Al_{1.044}Fe^{3+}_{0.413}Ti_{0.045}V_{0.009}$	54.1(3)	54.7	2.031(2)	2.031
Z	$Al_{4.806}Fe^{3+}_{0.152}Mg_{1.042}$	78*	78.9	1.933(2)	1.933
T	$Si_{6.000}$	84*	84	1.620(2)	1.620
W	$OH_{0.501}O_{0.499}$	8.0*	8.0		
	Magnesio-lucchesiite (rim)				
X	$Ca_{0.491}Sr_{0.021}Na_{0.415}K_{0.036}\square_{0.037}$	16.0(2)	15.9	2.654(4)	
Y	$Fe^{2+}_{0.945}Mg_{0.750}Al_{0.737}Fe^{3+}_{0.404}Ti_{0.146}V_{0.018}$	56.8(3)	57.3	2.050(3)	2.050
Z	$Al_{4.749}Fe^{3+}_{0.137}Mg_{1.115}$	78*	78.7	1.935(3)	1.935
T	$Si_{6.000}$	84*	84	1.621(2)	1.620
W	$O_{0.810}F_{0.184}OH_{0.006}$	8.2(1)	8.2		

* Scattering for the fixed site population.

Table 6. Bond-valence analysis for the Budniki tourmalines.

	X	Y	Z	B	T	BVS
Dravite–oxy-dravite						
O1		$0.437^{\times 3\rightarrow}$				1.312
O2	$0.155^{\times 3\downarrow}$	$0.419^{\times 2\rightarrow\downarrow}$		1.014		2.008
O3		0.319	$0.405^{\times 2\rightarrow}$			1.130
O4	$0.064^{\times 3\downarrow}$				$0.992^{\times 2\rightarrow}$	2.047
O5	$0.077^{\times 3\downarrow}$				$0.958^{\times 2\rightarrow}$	1.993
O6		$0.425^{\times 2\downarrow}$	0.515		1.045	1.984
O7			0.506		1.052	1.990
			0.432			
O8			0.511	$0.989^{\times 2\downarrow}$		1.968
			0.468			
BVS	0.887	2.445	2.838	2.992	4.046	
valence	0.990	2.518	2.826	3.000	4.000	
Magnesio-lucchesiite						
O1		$0.448^{\times 3\rightarrow}$				1.344
O2	$0.198^{\times 3\downarrow}$	$0.402^{\times 2\rightarrow\downarrow}$		0.964		1.966
O3		0.295	$0.411^{\times 2\rightarrow}$			1.117
O4	$0.100^{\times 3\downarrow}$				$0.977^{\times 2\rightarrow}$	2.055
O5	$0.121^{\times 3\downarrow}$				$0.941^{\times 2\rightarrow}$	2.003
O6		$0.426^{\times 2\downarrow}$	0.515		1.053	1.993
O7			0.497		1.061	1.983
			0.425			
O8			0.509	$0.997^{\times 2\downarrow}$		1.974
			0.468			
BVS	1.256	2.398	2.825	2.959	4.032	
valence	1.475	2.484	2.814	3.000	4.000	

Bond valence sums (BVS) were calculated using the equation $S = \exp[(R_0 - R)/B]$, where R_0 and B are bond-valence parameters derived by Gagné and Hawthorne (2015), and R is the refined bond length.

The Y and Z site populations were optimised for six possible occupants: Mg, Fe^{2+}, Al, Fe^{3+}, V^{3+} and Ti^{4+}, assuming that the Z sites can be filled by Al, Mg and Fe^{3+}, and the Y sites also by Fe^{2+} and the two remaining trace constituents. The Z-site population was determined from the following relationships:

(1) $Al + Mg + Fe^{3+} = 6$ apfu
(2) $13Al + 12Mg + 26Fe^{3+}$ = total optimised site-scattering value (78.93 vu for dravite–oxy-dravite, and 78.66 vu for magnesio-lucchesiite)
(3) $0.535Al + 0.72Mg + 0.645Fe^{3+} = (6 \times 1.9333) - (5 \times 1.36) - 1.38$ (dravite–oxy-dravite), or $(6 \times 1.9349) - (5 \times 1.36) - 1.38$ (magnesio-lucchesiite),

where Al, Mg and Fe^{3+} denote contents of the cations at the Z sites in the formal units; 13, 12 and 26 = numbers of electrons in the element constituents; 0.535, 0.72 and 0.645 = radii of the respective cations according to Shannon (1976), 1.36 and 1.38 = radii of $^{(3)}O^{2-}$ and $^{(4)}O^{2-}$ anions bonded to the *Z* cation (*ibidem*); 78.93 or 78.66 = the optimised total Z-site scattering; and 1.9333 and 1.9349 = the refined <Z–O> mean distances. The Y-site population was estimated from differences. Because the total scattering for the refined (Y + Z) site populations, $Mg_{1.710(25)}Fe_{1.290(25)}Al_{6.000}$ equal to 132.06(25) vu for dravite–oxy-dravite, and $Mg_{1.515(34)}Fe_{1.485(34)}Al_{6.000}$ equal to 134.79(34) vu for magnesio-lucchesiite (Table 3), differ slightly from the calculated numbers of electrons derived from the microprobe-measured raw populations (135.19 and 137.09 vu, respectively), both site-scattering values were optimised to 133.63 and 135.94 vu as averages between the microprobe determined and refined ones. The latter differ from the original refined values by somewhat less than 2 S.D. (Table 3), and the differences in the optimised MgO, FeO, Al_2O_3 and

https://doi.org/10.1180/mgm.2022.114 Published online by Cambridge University Press

TiO_2 amounts are also in the range of 2–3 S.D. of the microprobe spot analyses (Table 1).

These assumptions allowed the optimisation of the Y- and Z-site populations of the dravite–oxy-dravite crystal of: $^{Y}[(Fe^{2+}_{0.810}Mg_{0.680})_{\Sigma 1.490}(Al_{1.044}Fe^{3+}_{0.413}V_{0.009})_{\Sigma 1.465}Ti_{0.045}]_{\Sigma 3}{}^{Z}(Al_{4.806}Mg_{1.042}Fe^{3+}_{0.152})_{\Sigma 6}$ for which the calculated Y- and Z-site scatterings are equal to 54.7 and 78.9 vu, corresponding to the optimised value of 133.6 vu, and the calculated <Y–O> and <Z–O> distances 2.031 and 1.933 Å corresponding to the refined values (Table 5). Analysis of bond-valence sums at the Y and Z sites (Table 6) indicates 2.45 and 2.84 vu, respectively, which are very close to averaged valences of the respective complex cations, 2.52 and 2.83 vu. Differences between the respective values: +0.07 and –0.01 vu, fit well confirming the accuracy of the bond-valence method.

Similar optimisation in case of magnesio-lucchesiite led to the following Y- and Z-site populations: $^{Y}[(Fe^{2+}_{0.945}Mg_{0.750})_{\Sigma 1.695}(Al_{0.737}Fe^{3+}_{0.404}V_{0.018})_{\Sigma 1.159}Ti_{0.146}]_{\Sigma 3}{}^{Z}(Al_{4.749}Mg_{1.115}Fe^{3+}_{0.137})_{\Sigma 6}$, for which the calculated Y and Z site scatterings are equal to 57. 3 and 78.7 vu corresponding to the optimised value of 135.9 vu, and the calculated <Y–O> and <Z–O> distances of 2.050 and 1.935 Å correspond to the refined ones (Table 5). Analysis of the bond-valence sums at the Y and Z sites (Table 6) indicated 2.40 and 2.82 vu, respectively, which are again very close to averaged valences of the respective complex cations, 2.48 and 2.81 vu.

The W site occupancy was fixed as $O_{1.00}$ in dravite–oxy-dravite on the basis of microprobe analysis, and refined as $O_{0.79(13)}F_{0.21(13)}$ in magnesio-lucchesiite. In the case of dravite–oxy-dravite, the occupancy indicates F absence in the crystal whereas for magnesio-lucchesiite, the refined occupancy agrees with microprobe analysis and the optimised F content.

Genetic implications

The discovery of magnesio-lucchesiite at Budniki, in the Polish Karkonosze Mountains, represents the third documented occurrence of this rare Ca-dominant oxy-tourmaline species worldwide. Magnesio-lucchesiite was previously found in two independent geological occurrences: a lamprophyre dyke that cross-cuts tourmaline-rich metapelites within the exocontact of the O'Grady Batholith, Northwest Territories, Canada, and in hydrothermal veins embedded in meta-serpentinites within the contact aureole of the Monte Capanne intrusion at the San Piero in Campo village, Elba Island, Italy (Scribner *et al.*, 2021). A further finding of this peculiar tourmaline species was mentioned by Krmíček *et al.* (2021) in the locality of Černá, in the Český Krumlov Unit in Moldanubicum, Czech Republic. Both in the type and co-type localities, magnesio-lucchesiite is associated with Ca- and Mg-bearing ultrabasic rocks metasomatised by B-rich fluids, whereas in the Czech locality, the mineral is associated with metacarbonates occurring in mica schists and gneisses of the Český Krumlov unit.

The occurrence at Budniki corresponds well to the magnesio-lucchesiite type and cotype localities. Its genesis relates to the Variscan prograde and early retrograde metamorphism preceding the intrusion of the Karkonosze granite. Pressure–temperature conditions of prograde metamorphism for the Budniki amphibolites were estimated to be ~6 Kb and 600–550°C. During retrogression, pressure decreased to 2–3 Kb, and temperature to 540–510°C at an early stage, increasing to 620–635°C at the contact metamorphism peak, followed by a further retrogression down to 510–470°C (Mochnacka *et al.*, 2008; Oberc-Dziedzic *et al.*, 2010). At prograde metamorphism stage, boron with other mobile components, e.g. SiO_2, could have been released mainly from sedimentary protoliths of the Velká Upá mica schists and migrated as aqueous fluids infiltrating into the surrounding rocks (Dutrow *et al.*, 1999). We suppose that dravite–oxy-dravite core tourmaline was formed by interaction of the fluids with the rocks in which the veins were emplaced. Such metasomatic interaction could have supplied, successively, some amounts of Mg, Fe, Al, Ti, and also Sr, V, Cr, Ni and Co in traces, to the growing tourmaline crystals. Some of the constituents are present in amphibolite in the form of ilmenite–rutile–titanite aggregates, and as disseminated Ni–Co–Fe sulfide and sulfoarsenide ores typical for basic magmas. These B-bearing fluids could have been also sources for other quartz–tourmaline veins and veinlets in the Karkonosze granite metamorphic envelope of the Kowary region, for example, at the Wołowa Góra Mt. near to the Budniki camp, containing oxy-dravite, fluor-dravite and dravite (Lis *et al.*, 1965; Pieczka *et al.*, 2018).

Similarly to the type occurrence, the magnesio-lucchesiite from Budniki occurs as overgrowths on the partially leached dravite–oxy-dravite core. There is an abrupt increase in Ca and F with only minor changes in other chemical parameters. The occurrence of magnesio-lucchesiite as a thin outer zone may suggest that the only source of boron at this stage is that released by dissolving dravite–oxy-dravite. Some of these features seem to be typical for magnesio-lucchesiite occurrences: the enrichment in TiO_2 reaches 1.92 wt.% in the type locality and 1.62 wt.% at Černá, while at Budniki dravite is enriched in TiO_2 up to 1.60 wt.%, and magnesio-lucchesiite to 1.30 wt.%. Also, all described crystals are enriched in V and Cr. In all the cases, these features reflect the chemical composition of the host rocks. Finally, the chemistry of the fluids is partly documented by abundant calcite fillings in the latest microtectonic fissures that cut the quartz–tourmaline veinlets, and more rarely by fluorite.

Conclusions

Tourmaline from quartz veinlets that cross-cut amphibolite hosted by the Velká Upá mica schists at the Budniki camp in the eastern envelope of the Karkonosze granite near the Kowary town, SW Poland, evolves from oxy-dravite to magnesio-lucchesiite in prograde Variscan metamorphism and early retrogression stages. The species grown from B-bearing metamorphic fluids derived from the surrounding mica schist protoliths, which interacted with the amphibolite. Evolution of the fluids with the crystallisation progression and temperature decrease led to the replacement of dravite–oxy-dravite core tourmaline by magnesio-lucchesiite, forming crystals with rims richer in Ca and F. The origin of these differences is not clear: Ca and F may originate both from the amphibole or be derived from the surrounding Velká Upá group pelitic protoliths of mica schists interbedded with calcareous sediments.

Acknowledgements. We greatly thank Peter Leverett and two anonymous reviewers for their constructive comments on the manuscript. This study was supported by the National Science Centre (Poland) grant 2017/27/N/ST10/01579 to M.S. and AGH University of Science and Technology grant 16.16.140.315.

Competing interests. The authors declare none.

Supplementary material. To view supplementary material for this article, please visit https://doi.org/10.1180/mgm.2022.114

References

Berryman E.J., Wunder B., Wirth R., Rhede D., Schettler G., Franz G. and Heinrich W. (2015) An experimental study on K and Na incorporation in dravitic tourmaline and insight into the origin of diamondiferous tourmaline from the Kokchetav Massif, Kazakhstan. *Contributions to Mineralogy and Petrology*, **169**, 1–16.

Berryman E.J., Wunder B., Rhede D., Schettler G., Franz G. and Heinrich W. (2016) P–T–X controls on Ca and Na distribution between Mg–Al tourmaline and fluid. *Contributions to Mineralogy and Petrology*, **171**, 1–14.

Biernacka J. (2019) Insight into diagenetic processes from authigenic tourmaline: An example from Carboniferous and Permian siliciclastic rocks of western Poland. *Sedimentary Geology*, **389**, 73–90.

Borkowska M., Hameurt J. and Vidal P. (1980) Origin and age of Izera gneisses and Rumburk granites in the Western Sudetes. *Acta Geologica Polonica*, **30**, 121–146.

Dolomanov O.V., Bourhis L.J., Gildea R.J., Howard J.A.K. and Puschmann H. (2009) OLEX2: a complete structure solution, refinement and analysis program. *Journal of Applied Crystallography*, **42**, 339–341.

Dutrow B.L. and Henry D.J. (2016) Fibrous tourmaline: a sensitive probe of fluid compositions and petrologic environments. *The Canadian Mineralogist*, **54**, 311–335.

Dutrow B.L., Foster C.T. and Henry D.J. (1999) Tourmaline-rich pseudomorphs in sillimanite zone metapelites: Demarcation of an infiltration front. *American Mineralogist*, **84**, 794–805.

Ertl A., Marschall H.R., Giester G., Henry D.J., Schertl H.P., Ntaflos T., Luvizotto G.L., Nasdala L. and Tillmans E. (2010) Metamorphic ultrahigh-pressure tourmaline: Structure, chemistry, and correlations to PT conditions. *American Mineralogist*, **95**, 1–10.

Gagné O.C. and Hawthorne F.C. (2015) Comprehensive derivation of bond-valence parameters for ion pairs involving oxygen. *Acta Crystallographica*, **B71**, 562–578.

Henry D.J. and Dutrow B.L. (1996) Metamorphic tourmaline and its petrologic applications. Pp. 503–557 in: *Boron: Mineralogy, Petrology, and Geochemistry* (Lawrence M. Anovitz and Edward S. Grew, editors). Reviews in Mineralogy, **33**. Mineralogical Society of America, Washington DC.

Henry D.J. and Dutrow B.L. (2012) Tourmaline at diagenetic to low-grade metamorphic conditions: Its petrologic applicability. *Lithos*, **154**, 16–32.

Henry D.J. and Guidotti C.V. (1985) Tourmaline as a petrogenetic indicator mineral: an example from the staurolite-grade metapelites of NW Maine. *American Mineralogist*, **70**, 1–15.

Henry D.J., Novák M., Hawthorne F.C., Ertl A., Dutrow B.L., Uher P. and Pezzotta F. (2011) Nomenclature of the tourmaline-supergroup minerals. *American Mineralogist*, **96**, 895–913.

Ilnicki S. (2011) Variscan prograde PT evolution and contact metamorphism in metabasites from the Sowia Dolina, Karkonosze-Izera massif, SW Poland. *Mineralogical Magazine*, **75**, 185–212.

Korytowski A., Dörr W. and Żelaźniewicz A. (1993) U-Pb dating of (meta) granitoids in the NW Sudetes (Poland) and their bearing on tectonostratigraphic correlation. *Terra Nova*, **5**, 331–332.

Krmíček L., Novák M., Trumbull R., Cempírek J. and Huzar S. (2021) Boron isotopic variations in tourmaline from metacarbonates and associated calc-silicate rocks from the Bohemian Massif: constraints on boron recycling in the Variscan orogen. *Geoscience Frontiers*, **12**, 219–230.

Kröner A., Jaeckel P., Hegner E. and Opletal M. (2001) Single zircon ages and whole-rock Nd isotopic systematics of early Palaeozoic granitoid gneisses from the Czech and Polish Sudetes (Jizerské hory, Krkonoše Mountains and Orlice-Sněžník Complex). *International Journal of Earth Sciences*, **90**, 304–324.

Kryza R. and Mazur S. (1995) Contrasting metamorphic paths in the SE part of the Karkonosze-Izera block (Western Sudetes, SW Poland). *Neues Jahrbuch fur Mineralogie-Abhandlungen*, **169**, 157–192.

Kryza R., Pin C., Oberc-Dziedzic T., Crowley Q.G. and Larionov A. (2014) Deciphering the geochronology of a large granitoid pluton (Karkonosze Granite, SW Poland): an assessment of U–Pb zircon SIMS and Rb–Sr whole rock dates relative to U–Pb zircon CA–ID–TIMS. *International Geology Review*, **56**, 756–782.

Kusiak M.A., Williams I.S., Dunkley D.J., Konečný P., Słaby E. and Martin H.M. (2014) Monazite to the rescue: U–Th–Pb dating of the intrusive history of the composite Karkonosze pluton, Bohemian Massif. *Chemical Geology*, **364**, 76–92.

Lis J., Stępniewski M. and Sylwestrzak H. (1965) Brannerite and co-existing minerals in the quartz vein from Wołowa Góra Mt. Near Kowary (Sudetes). *Biuletyn Instytutu Geologicznego*, **193**, 203–223 [in Polish only].

Machowiak K. and Armstrong R. (2007) SHRIMP U–Pb zircon age from the Karkonosze granite. *Mineralogia – Special Papers*, **31**, 193–196.

Mazur S. (1995) Structural and metamorphic evolution of the country rocks at the eastern contact of the Karkonosze granite in the southern Rudawy Janowickie Mts and Lasocki Range. *Geologia Sudetica*, **29**, 31–98 [in Polish only with English summary].

Mazur S., Aleksandrowski P., Kryza R. and Oberc-Dziedzic T. (2006) The Variscan Orogen in Poland. *Geological Quarterly*, **50**, 89–118.

Mochnacka K., Oberc-Dziedzic T., Mayer W. and Pieczka A. (2008) Ti remobilization and sulphide/sulphoarsenide mineralization in amphibolites: effect of granite intrusion (the Karkonosze-Izera Massif, SW Poland). *Geological Quarterly*, **52**, 349–368.

Oberc-Dziedzic T. (1988) The development of gneisses and granites in the eastern part of the Izera crystalline unit in the light of textural investigations. *Acta Universitatis Wratislaviensis*, **997**, 1–184.

Oberc-Dziedzic T., Kryza R., Klimas K., Fanning M.C. and Madej S. (2005) Gneiss protolith ages and tectonic boundaries in the NE part of the Bohemian Massif (Fore-Sudetic Block, SW Poland). *Geological Quarterly*, **49**, 363–378.

Oberc-Dziedzic T., Kryza R., Mochnacka K. and Larionov A. (2010) Ordovician passive continental margin magmatism in the Central-European Variscides: U–Pb zircon data from the SE part of the Karkonosze-Izera Massif, Sudetes, SW Poland. *International Journal of Earth Sciences* (*Geologishe Rundschau*), **99**, 27–46.

Oliver G.J.H., Corfu F. and Krogh T.E. (1993) U-Pb ages from SW Poland: evidence for a Caledonian suture zone between Baltica and Gondwana. *Journal of the Geological Society*, **150**, 355–369.

Pasero M. (2022) The New IMA List of Minerals – A Work in Progress – Updated: July 2022. http://cnmnc.main.jp/IMA_Master_List_(2022-07).pdf

Pieczka A., Ertl A., Sęk M.P., Twardak D., Zelek S., Szełęg E. and Giester G. (2018) Oxy-dravite from Wołowa Góra Mountain, Karkonosze massif, SW Poland: Crystallochemical and structural studies. *Mineralogical Magazine*, **82**, 913–928.

Pin C., Kryza R., Oberc-Dziedzic T., Mazur S., Turniak K. and Waldhausrová J. (2007) The diversity and geodynamic significance of Late Cambrian (ca. 500 Ma) felsic anorogenic magmatism in the northern part of the Bohemian Massif: A review based on Sm-Nd isotope and geochemical data. *The Evolution of the Rheic Ocean: From Avalonian-Cadomian Active Margin to Alleghenian-Variscan Collision*, **423**, 209–229.

Scribner E.D., Cempírek J., Groat L.A., Evans R.J., Biagioni C., Bosi F., Dini A., Hålenius U., Orlandi P. and Pasero M. (2021) Magnesio-lucchesiite, $CaMg_3Al_6(Si_6O_{18})(BO_3)_3(OH)_3O$, a new species of the tourmaline supergroup. *American Mineralogist*, **106**, 862–871.

Shannon R.D. (1976) Revised effective ionic radii and systematic studies of interatomic distances in halides and chalcogenides. *Acta Crystallographica*, **A32**, 751–767.

Sheldrick G.M. (2015a) SHELXT - Integrated space-group and crystal-structure determination. *Acta Crystallographica*, **A71**, 3–8.

Sheldrick G.M. (2015b) Crystal structure refinement with SHELXL. *Acta Crystallographica*, **C71**, 3–8.

Slack J.F. and Trumbull R.B. (2011) Tourmaline as a recorder of ore-forming processes. *Elements*, **7**, 321–326.

van Hinsberg V.J., Schumacher J.C., Kearns S., Mason P.R. and Franz G. (2006) Hourglass sector zoning in metamorphic tourmaline and resultant major and trace-element fractionation. *American Mineralogist*, **91**, 717–728.

van Hinsberg V.J., Henry D.J. and Dutrow B.L. (2011) Tourmaline as a petrologic forensic mineral: A unique recorder of its geologic past. *Elements*, **7**, 327–332.

Warr L.N. (2021) IMA–CNMNC approved mineral symbols. *Mineralogical Magazine*, **85**, 291–320.

Żaba J. (1984) Genesis and metamorphic evolution of gneisses and granitoids of the Izerski Stóg massif (Western Sudetes). *Geologia Sudetica*, **19**, 90–190.

https://doi.org/10.1180/mgm.2022.114 Published online by Cambridge University Press